

Modeling the operating conditions of solar concentrator systems

G. Groot Gregory^{*a} and R. John Koschel^b
Lambda Research Corporation

^a25 Porter Road, Littleton, MA 01460-1434

^b8230 East Broadway, Suite E2, Tucson, AZ 85710

ABSTRACT

Converting energy from the sun's radiation into electrical current has been a reality for over 40 years but the efficiency derived from these devices has been low and not economically practical. With recent developments in solar cell technology, including multi-junction cells, conversion efficiency of nearly 40% has been demonstrated in the laboratory. The efficiency gain is due to the structure of the cell coupled with optics used to concentrate the sunlight onto the device. The concentrator design requires that the cell be uniformly illuminated to achieve the highest efficiency. Optical analysis software is used in the design and simulation of the system comprised of the solar radiation, optical concentrator and solar cell. This paper will describe the modeling of these concentrators and illustrate how the simulation can provide improved designs to achieve high illumination uniformity.

Keywords: Software, illumination, simulation, solar energy, photovoltaic cell, concentrator, Fresnel lens

1. INTRODUCTION

Systems that employ solar radiation are receiving more attention in recent years, such as photovoltaics for energy production, solar water heating, daylighting, and so forth. The simulation of solar cells, especially ones that employ the improving technology of multi-junction (MJ) photovoltaic cells (PVs), is the focus of this paper. Simple silicon PVs typically employ surface receivers since concentration provided little if negligible improvement without substantial additional costs and system complexity. Commercial silicon PV modules provide conversion efficiency in the range of 10% to 15%. In order to make solar energy systems more cost efficient and thus attractive to industrial development, the solar cell efficiency must be improved, which is the drive behind multi-junction systems. MJ PV modules in the commercial sector are providing over 30% efficiency,¹ and conversion efficiency over 37% has been seen in the laboratory.² MJ PVs are limited in their size and their performance degrades with a lack of uniformity across the active area.³ Additionally, MJ PVs tend to provide better optical-to-electrical conversion over a range of concentration above the nominal provided by the direct solar radiation. This concentration provides a numeric metric in multiples of nominal solar radiation, called Suns, where 1 Sun is equal to 1000 W/m². Thus, MJ PVs require the integration of concentrators, including but not limited to, reflective troughs or wells such as compound parabolic concentrators (CPCs) and refractive elements such as Fresnel lenses, imaging or nonimaging.

Software tools, such as TracePro®,⁴ can be used to design the concentrators in order to improve the transfer efficiency to the receiver, the concentration, and the uniformity across the receiver. All of these steps are within the repertoire of optical designers and nonimaging software codes, but such design aspects leave out important considerations of the source, receiver, and environmental conditions, such as:

- Position of the system in latitude and longitude,
- Date and time at the prescribed location,
- Atmospheric conditions that degrade solar radiation,
- Tracking of the concentrator PV system,
- Receiver optical-to-electrical conversion efficiency, and
- Non-uniformity performance degradation at the receiver.

* Groot.Gregory@osa.org; phone 1 978 486-0766; fax 1 978 486-0755; www.lambdares.com

By including the above in the simulation model, one can actually optimize performance of the PV system in light of operation conditions. Such tools are necessary to predict actual performance in the field. Herein we investigate the inclusion of several of these operating conditions, including the position of the system, date and time of operation, atmospheric conditions, tracking, and receiver conversion efficiency. Receiver irradiance non-uniformity requires additional input from the PV manufacturers prior to implementation. Note that the goal of this work is to provide a set of tools to ease the development and analysis of solar energy systems. With the inclusion of operating conditions through a simple user interface, the designer can focus on optimization of the system performance, rather than setting up the model of the source and its operating conditions.

In the next section the characteristics of the system model are presented. There are sections devoted to the atmospheric model, the source model, the receiver model, and the optical component models. Following that are two sections devoted to systems employing refractive Fresnel lenses and reflective nonimaging CPCs. Finally, this paper ends with conclusions.

2. OPERATION CHARACTERISTICS OF THE SYSTEM MODEL

There are several aspects of the PV system that must be modeled in order to contend for operation in the field. They are: source model, receiver model, atmospheric model, and optical component models. Each of these elements is described in the following subsections.

2.1. Source model

The source model is comprised of two components: direct solar radiation and indirect solar radiation from atmospheric scattering. Both source components are dependent on a number of parameters, including: latitude, longitude, and elevation of the concentrator; date and time of the year; spectrum or spectra of interest; and the angular subtense of the solar disc and the scattered light. Within this paper three locations are investigated: Strasbourg, France (i.e., the location of the Photonics Europe 2006 Conference); Littleton, MA (i.e., the location of the Lambda Research US East coast office); and Tucson, AZ (i.e., the location of the Lambda Research US West coast office). Table 1 provides the latitude, longitude, and elevation for these three locations. We also provide results for the remainder of this paper for one day of the year: 6 April 2006, which is the day that this paper is presented at the conference. The spectra of interest are limited to that of the effectiveness of conversion at the receiver; however, it is noted in the next subsection that the spectral components of the source can be integrated into the conversion efficiency at the receiver. In other words, a single wavelength can be used to model the system performance by including the receiver conversion efficiency into the target absorption model. Albeit, this assumption removes any chromatic aberration effects within the system, but these prove to be negligible for refractive concentrators using Fresnel lenses² and reflective systems. The direct radiation is modeled as a Lambertian disc that subtends 9.3 mrad at the Earth surface, while the indirect radiation is modeled as a hemisphere emitting internally into 2π steradians. The randomly generated rays are assigned flux dependent on the operating conditions, including atmospheric conditions (see Section 2.3 for further discussion). The rays are directed over a prescribed area centered on the origin, where the concentrating optics are placed.

Table 1. Latitude, longitude, and elevation for the three locations studied herein: Strasbourg, France; Littleton, MA; and Tucson, AZ.

Location	Longitude (°)	Latitude (°)	Elevation (m)
Strasbourg, France	48.58 N	7.75 E	153
Littleton, MA, USA	42.55 N	71.47 W	79
Tucson, AZ, USA	32.21 N	110.92 W	759

2.2. Receiver model

The receiver for this study is the Spectrolab Triple-Junction Terrestrial Concentrator Solar Cell (see Ref. 1). This PV is comprised of three thin films made of GaInP₂, GaAs, and Ge. Each of the films absorbs incident radiation in different spectral bands, with the peak absorption for GaInP₂ around 520 nm, the peak for GaAs at 800 nm, and the broad Ge

absorption band centered at about 1200 nm. The PV cell size is designed per customer request, but when mounted on a ceramic substrate the typical active area size is 10 mm by 10 mm. This size is used for the remainder of the paper. The spectral absorption characteristics, coatings on the active area, and other PV parameters that affect optical-to-electrical conversion can be modeled individually; however, this process is lengthy and requires ray tracing over several wavelength bands. Rather, a conversion model based on the measured performance of these solar cells can be integrated into the simulation. Figure 1 shows the conversion efficiency as a function of the logarithm of the local number of Suns concentrated onto the active area of the PV cell. Thus, by making the active surface in the software model a perfect absorber, the curve presented in Fig. 1 dictates the optical-to-electrical conversion efficiency while including spectral, quantum efficiency, and coating effects. This step greatly simplifies the modeling requirements, while also providing the expected electrical power that is generated by the solar cell. The conversion efficiency could be determined by a lookup table, but a better approach is to model the data curve in Fig. 1 by a polynomial, such that optical-to-electrical conversion can be integrated seamlessly into the model,

$$\eta_c = \begin{cases} \sum_{i=0}^6 a_i (\log E_{Suns})^i & E_{Suns} \geq 1 \\ b_1 E_{Suns} & E_{Suns} \leq 1 \end{cases}, \quad (1)$$

where η_c is the optical-to-electrical conversion efficiency, E_{Suns} is the irradiance in the units of Suns (i.e., 1000 W/m²), the a_i coefficients are within the nonlinear response region above one Sun, and the b_1 coefficient is within the linear threshold response region of the PV. For this study, the fit, shown in Fig. 1, has the coefficients with numeric values of $a_6 = 3.7692E-04$, $a_5 = -2.2455E-03$, $a_4 = -2.0722E-03$, $a_3 = 2.9234E-02$, $a_2 = -5.2560E-02$, $a_1 = 5.1549E-02$, $a_0 = 2.5497E-01$, and $b_1 = 0.255$.

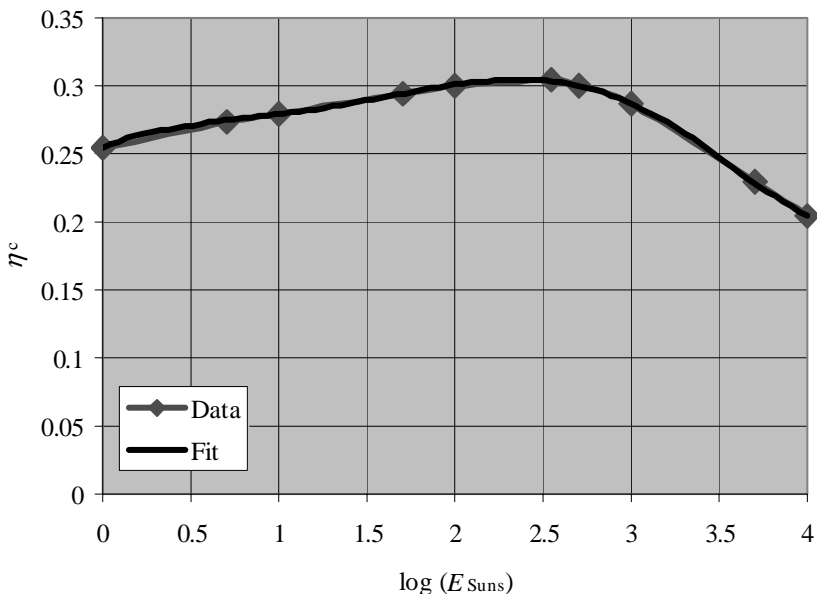


Figure 1. Plot of the optical-to-electrical conversion efficiency as a function of the logarithm of the irradiance in Suns. The data curve is from the datasheet of Ref. 1, while the fit is provided in Eq. (1).

2.3. Atmospheric model

The atmospheric conditions present during real-life operation of the solar-concentrating system can be included in the model. For example, the level of cloudiness, haze, smog, or other such conditions can be used to adjust the flux level of the two sources describe in Section 2.1. Figure 2 shows the nominal irradiances for the three locations on the date of 6 April 2006 as a function of the time. Note that three cases are shown for each location: sunny, partly cloudy, and cloudy.

The cloudy and sunny cases indicate limits to the range of irradiance as a function of time, while the partly cloudy case shows an averaging of the incident solar radiation. By averaging it is implied that over a finite time period the irradiance level will be on average the stated values. Of course the level of cloudiness between sunny and cloudy affects the irradiance, as would other conditions such as haze, precipitation, and so forth. The atmospheric conditions are used to adjust the flux emanating from the two sources in the software model. Additional filtering functions could also be integrated into the model between the source and the concentrator to contend for other conditions, such as haze, but to decrease the ray-tracing time, it is best to include such in the source models.

As can be seen in Fig. 2, the Tucson location provides the best irradiance in Suns on the Earth surface for sunny and partly cloudy conditions. In cloudy conditions all three sites tend to give about the same amount of solar radiation, with all of it due to indirect, scattered light.

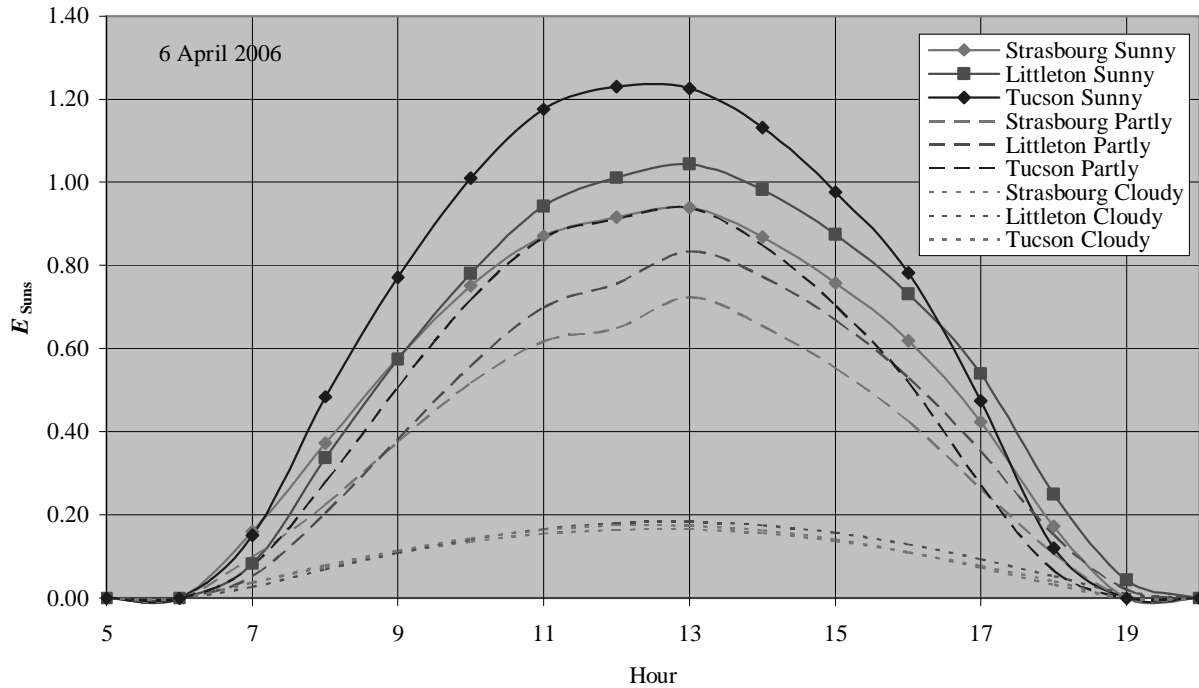


Figure 2. The irradiance in Suns for three atmospheric conditions; sunny, partly cloudy, and cloudy; as a function of the local hour on 6 April 2006.

2.4. Optical component models

The components in the model are assigned optical properties including materials and surfaces. For the refractive components the following properties apply:

- Material: acrylic ($n_d = 1.49309$) and
- Surfaces: bare.

For reflective surfaces the following properties apply:

- Material: acrylic ($n_d = 1.49309$) and
- Surfaces: Alanod Miro 2 ($R_{\text{spec}} = 90\%$, $R_{\text{diff}} = 5\%$ (BRDF $A = 0.01751$, BRDF $B = 0.1$, BRDF $g = 0.0$), and $A = 5\%$). A , B and g are scatter coefficient in the TracePro ABg model.

The PV is modeled as a perfect absorber and the atmosphere is modeled as lossless with $n = 1$.

3. REFRACTIVE FRESNEL LENS MODEL

A Fresnel lens was designed to transfer the incident radiation to the active area of the PV. The circular Fresnel lens has a radius of 0.5 m and a 400-mm focal length. A negative lens is added near the solar cell to increase the optical efficiency to the PV. A slight amount of defocus is added to the position of the solar cell in order to improve the uniformity over the active region. Note that the optical design of the system has not been optimized, which would be the focus of continued study. The model is setup such that the lens tracks the Sun during the day. Figure 3 shows a schematic of the configuration including a few incident rays. Note that some of the rays propagate via total internal reflection (TIR) through the Fresnel lens substrate. The colors of the rays indicate the flux transferred by each ray.

Figure 4 shows the irradiance in Suns when the Fresnel lens is included (left-hand axis) and when there is no concentrator optic (right-hand axis) for Tucson on 6 April 2006. Note that Tucson is used for the remainder of this study to highlight its improved performance for solar energy systems. The other locations would have similar results, but the concentration is reduced. Figure 4 shows a concentration of about 3500 when the Fresnel lens is used to transfer the solar radiation to the target. The small difference between the curves for the concentrator and direct cases is due to small pointing errors of the concentrator system within the software model. It was noted during the design stages that the Fresnel lens is quite sensitive to tracking errors. Such errors would be exasperated in real-life scenarios, which is one reason that the ultimate system must be tolerant to tracking errors. Figure 5 shows the effectiveness of the Fresnel lens concentrator by displaying the generated electrical power (left-hand axis) and the optical-to-electrical conversion efficiency (right-hand axis) for the Tucson location. Note that the generated electrical power is nearly over 100 W from the local hour range of 10 to 16, while the conversion efficiency is over 30%. Figure 6 shows the tolerance as a pointing error is introduced into the system. The FWHM of the distribution is about 0.6° , which indicates, as expected, that a slight tracking error leads to poor performance of the generated electrical power. Figure 7 shows the uniformity on the solar cell for two cases (a) a collimated beam of light from the solar disc and (b) inclusion of the solar divergence due to the 9.3 mrad angular subtense of the solar disc. Note that the uniformity for case (b), which matches the expected operation in the field, is better than that of case (a). This uniformity metric still needs to be integrated into the performance metric of optical-to-electrical conversion efficiency.

The lack of insensitivity in tracking or pointing error is a major reason that Fresnel lenses are not attractive concentrators for solar energy generation. Nonimaging Fresnel lenses improve performance,⁵ but alternate technology, such as reflectors, are more attractive.

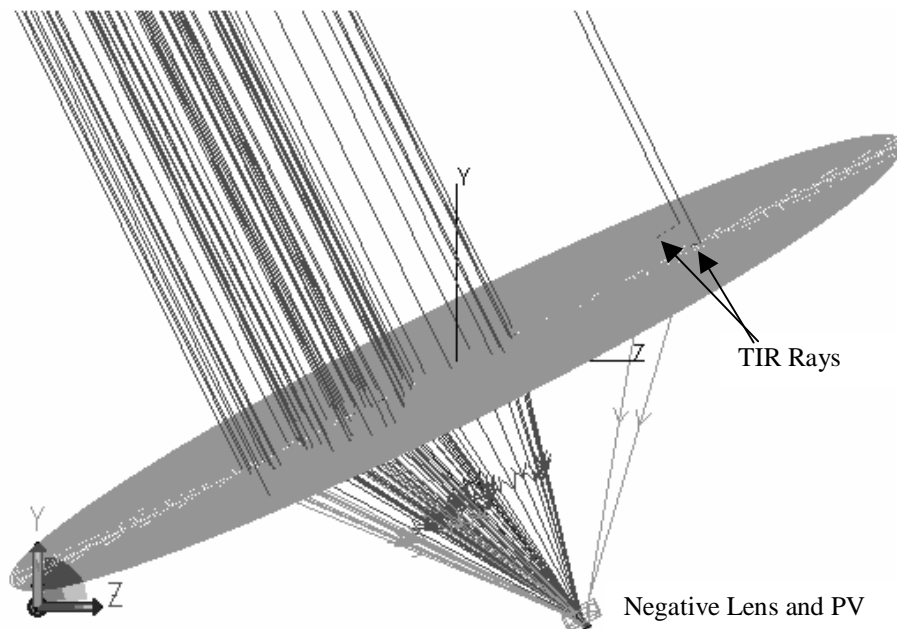


Figure 3. Schematic of the refractive Fresnel lens concentrator, showing a few rays propagating through the system.

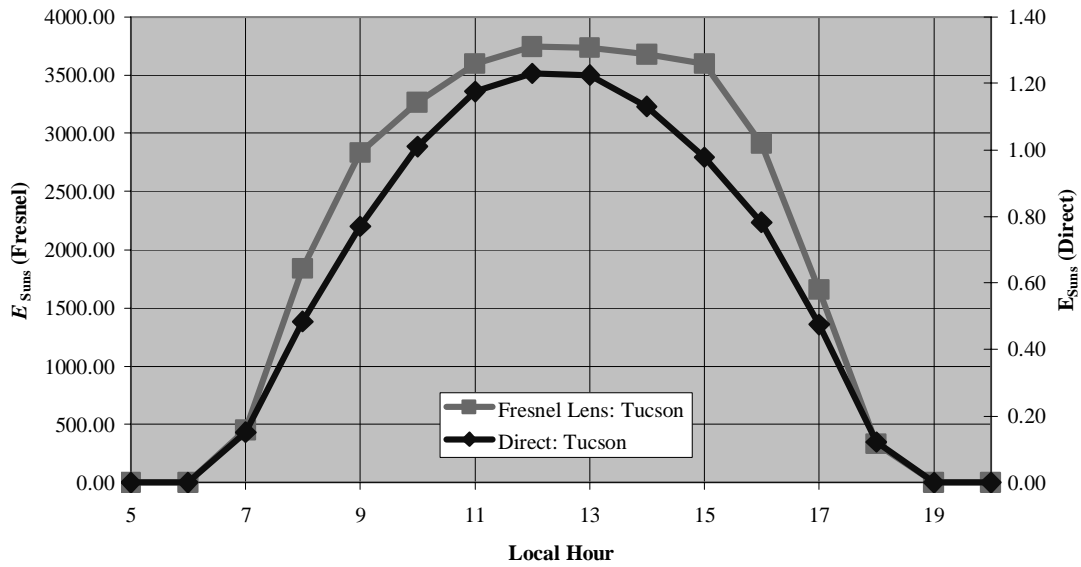


Figure 4. The irradiance in Suns using the Fresnel lens (left-hand axis) and the direct (right-hand axis) for Tucson on 6 April 2006.

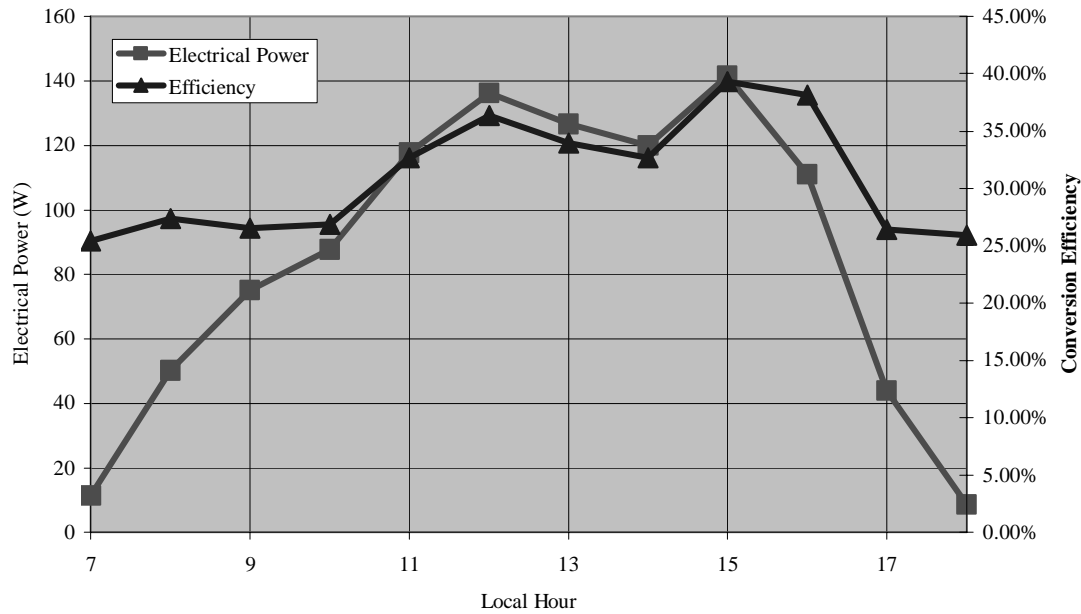


Figure 5. Generated electrical power (left-hand axis) and conversion efficiency (right-hand axis) as a function of local hour for the Fresnel lens case located in Tucson on 6 April 2006.

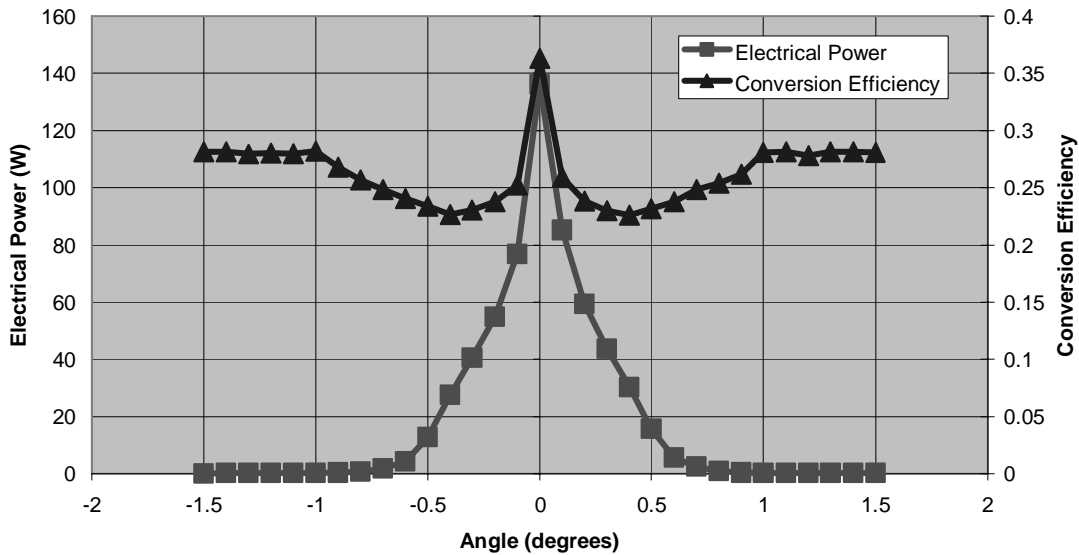


Figure 6. Tolerance of pointing error for generated electrical power (left-hand axis) and conversion efficiency (right-hand axis) at 12 local hour Tucson on 6 April 2006.

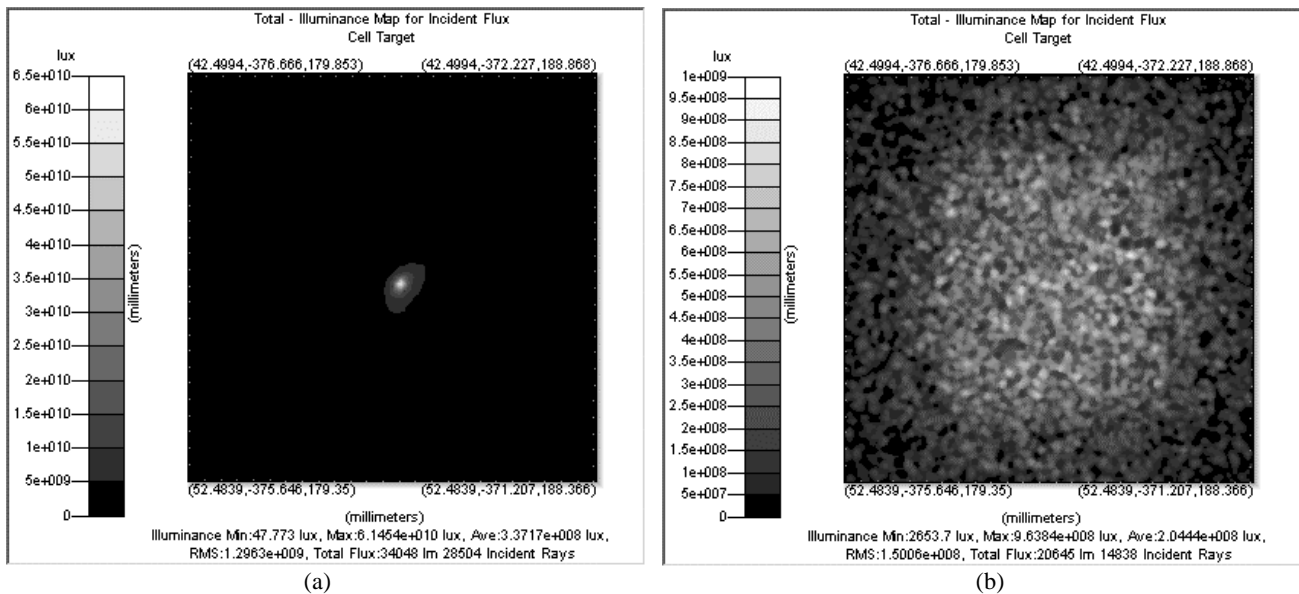


Figure 7. Effect of the solar model for (a) collimated beam of light from the solar disc and (b) inclusion of the solar divergence due to the 9.3 mrad angular subtense of the solar disc.

4. REFLECTIVE CPC MODEL

Reflective concentrators provide an attractive solution to contend with tracking errors while also maximizing transfer from the input aperture to the target (i.e., solar cell). Most reflective concentrators to date with the receiver being a photovoltaic cell are parabolic reflectors, but CPC-type devices have also been deployed.⁶ The difficulty with parabolic reflectors is their tracking demands, which are analogous to that of the Fresnel lens of the previous section. New methods are being investigated currently, including the simultaneous multiple surfaces (SMS) method and aplanatic

imaging systems that employ lightpipes near the solar cell.^{7,8} For additional discussion about reflective solar concentration methods, please see the references contained within Ref. 6. For the reflective concentrator model pursued within this paper, we investigated a rectangular aperture CPC (i.e., each of the two orthogonal axes of the CPC has the same prescribed acceptance angle). While this concentrator may not be optimal it will show the power generation capabilities, the conversion efficiency, and tolerances as a function of acceptance angle. Figure 8 shows a schematic of a CPC and some of the rays from a solar disc source.

The amount of incident optical power on the PV cell (left-hand axis) and generated electrical power from the PV cell (right-hand axis) for 2° and 5° acceptance angle CPCs that employ two-axis tracking are shown in Fig. 9. The data is shown as a function of local hour for Tucson on 6 April 2006. The slight discrepancy between the electrical and optical power curves is due to the integrated conversion efficiency performed at the detector. The detector is divided into 128 by 128 bins, and the conversion efficiency curve of Eq. (1) is applied to each of these bins separately. Thus, as a first step, PV irradiance nonuniformity is taken into account. Note that at noon with the 2° CPC, over 500 Suns is incident on the PV cell. This irradiance transforms into the generation of 15 W of electricity. Additionally, the level of electrical generation for the CPC in comparison to the Fresnel lens of the previous section is due to the reduction in the size of the entrance aperture. For the 2° CPC, the entrance aperture has an area of 0.082 m², while the Fresnel lens has an area of 0.79 m², which is a factor of 10 smaller. Scaling up the entrance aperture of the CPC to that of the Fresnel lens would predict an electrical generation of 150 W.

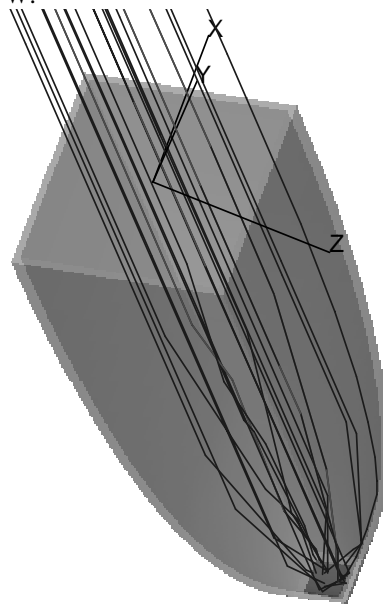


Figure 8. Schematic of the rectangular aperture CPC and reprehensive rays propagating to the PV cell.

Next, we investigate the transfer-conversion efficiency of the CPC-type device. The transfer-conversion efficiency includes the optical efficiency of the concentrator in the efficiency calculation. The transfer-conversion efficiency is given by

$$\begin{aligned}
 \eta &= \eta_t \eta_c \\
 &= \frac{P_{cell,opt}}{P_{in,opt}} \frac{P_{cell,elec}}{P_{cell,opt}} \\
 &= \frac{P_{cell,elec}}{P_{in,opt}},
 \end{aligned} \tag{2}$$

where η is the transfer-conversion efficiency, η_t the transfer (optical) efficiency, and the P terms indicating the power input (in), output (out), at the cell (cell) optical (opt), and electrical (elec). Figure 10 shows the two-axis tracking case with the power, both optical and electrical, (left-hand axis) and the transfer-conversion efficiency (right-hand axis) as a function of the acceptance angle of the CPC. Figure 11 shows the power results when there is no tracking of the device. The CPC is pointed to the zenith for this plot. The data is for local hour 13 (i.e., 1 pm) in Tucson on 6 April 2006. Additionally, within Fig. 10 a curve that follows $1/\sin^2\theta_a$, where θ_a is the acceptance angle of the CPC, is plotted. This sine function is analogous to the concentration that we would expect to see with such a reflector. Thus, the CPC is performing as expected when tracking is activated. As expected the power, both optical and electrical, decreases as the acceptance angle is increased due to the reduction in the entrance aperture area. The transfer-conversion efficiency is about 15% over the angular range plotted, which is a reduction from over 25% (conversion efficiency) due to the optical losses due to reflections. Note that this reduction is about 10%, which can be attributed to the specular loss of 10% per ray interaction with the Miro 2 surfaces of the reflector. With tracking removed, as per Fig. 11, the device performs poorly until the solar disc is within the field of view of the CPC. This view angle occurs around an acceptance angle of 30° . Below this angle there is some optical radiation incident on the PV due to reflector scatter of solar radiation and specular from the diffuse, sky radiation. The full difference in angle between the winter and summer suns is about 60° , which bears out the realization of the FOV cutoff around 30° .

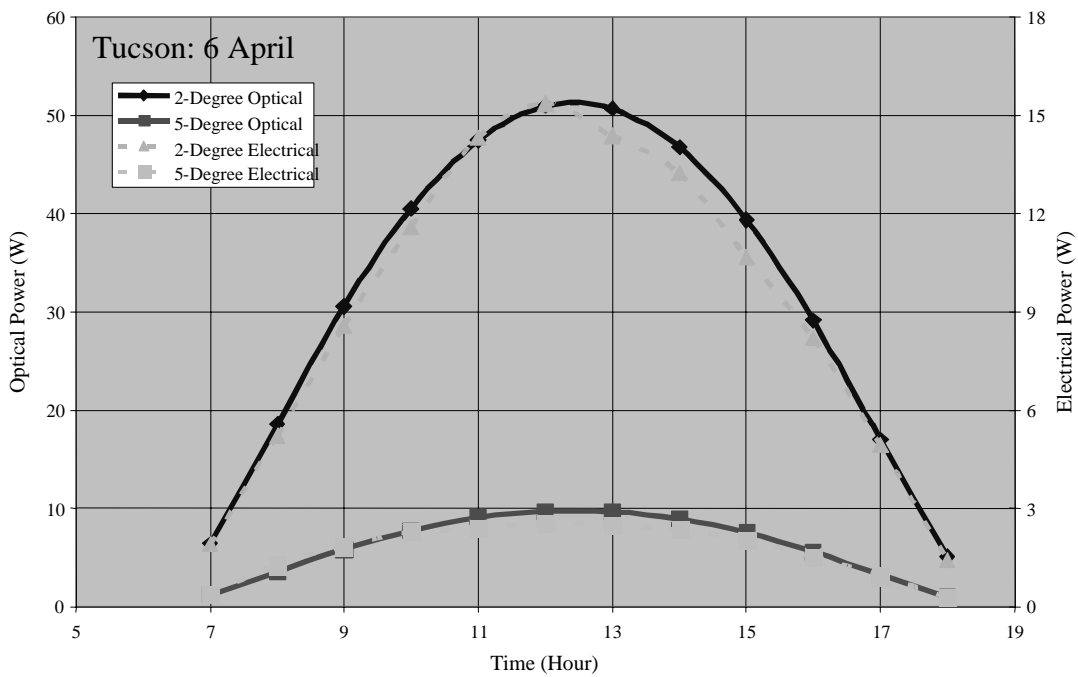


Figure 9. Optical (left-hand axis) and electrical (right-hand axis) power at the PV cell as a function of local hour at Tucson on 6 April 2006.

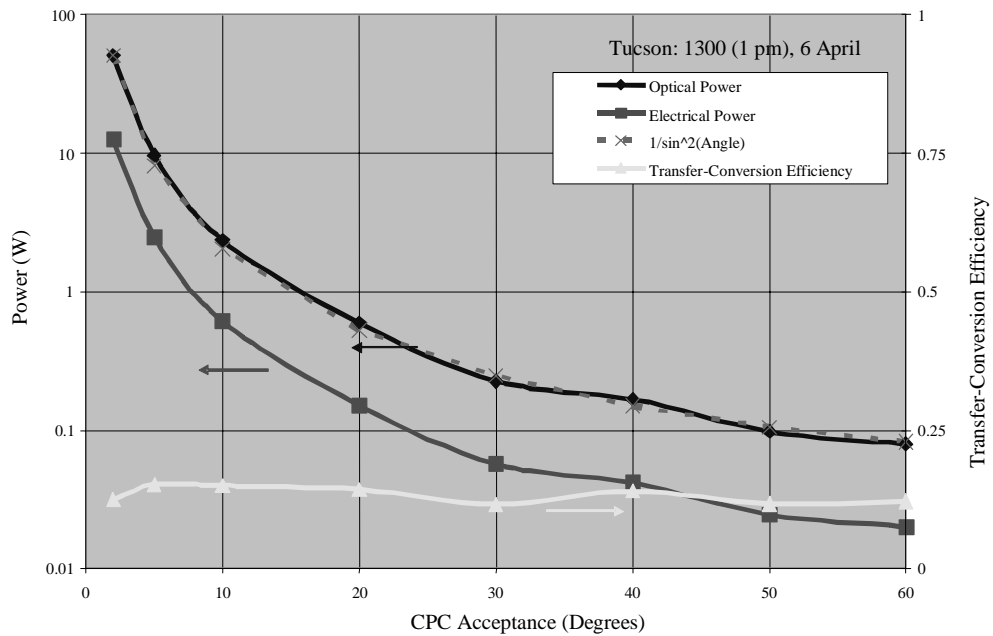


Figure 10. Power, optical and electrical, (left-hand axis) and transfer-conversion efficiency (right-hand axis) of the CPC system with two-axis tracking as a function of acceptance angle for Tucson at local time 13 on 6 April 2006.

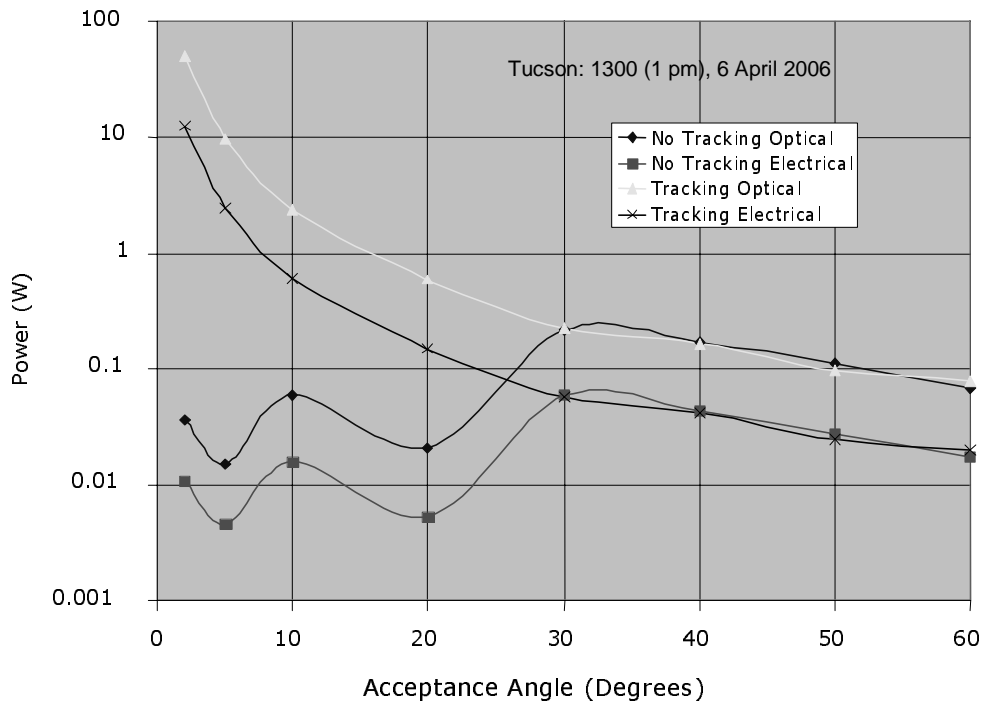


Figure 11. Power, optical and electrical, (left-hand axis) and transfer-conversion efficiency (right-hand axis) of the CPC system with no tracking as a function of acceptance angle for Tucson at local time 13 on 6 April 2006.

5. CONCLUSIONS

We have provided in this paper a systems approach to the design of solar energy concentrators. This process integrates into the design, optimization, and tolerance processes the operating conditions, such as the location of the concentrator system, tracking, the atmospheric conditions, the date and time of operation, and the optical characteristics of the system. Such treatments are going to be required to develop the state-of-the-art systems required for the inclusion of MJ PVs. These solar cells are limited in their size, and perform better when a certain, uniform concentration level (around 200 to 400 Suns) is obtained on the PV active region. The simulations contained herein do not include the degradation due to irradiance nonuniformity, but it is to be included in the future. Additionally, we plan to develop alternate source models that simplify the generation of the source model and make for more efficient ray tracing. One such example is the Bird model.

In conclusion, we have shown a method to integrate the complex system characteristics for the case of solar energy generation. Such a model allows optimization and tolerancing prior to expensive fabrication. Ultimately, these modeling capabilities will be included in software simulation codes, such as that of ref. 4.

Acknowledgments

Zack Rogers of Architectural Energy Corporation for motivation and source direction models.

REFERENCES

1. Spectrolab, "Triple Junction Terrestrial Concentrator Solar Cells," SpectrolabMJ.pdf Datasheet, www.spectrolab.com.
2. S. Kurtz and D. Friedman, "Photovoltaics: Lighting the Way to Brighter Future," *Opt. and Phot. News* 16(6), 30-35 (2005)
3. Ibid.
4. TracePro is a registered trademark of Lambda Research Corporation, see www.lambdare.com for more information about this software product.
5. R. Leutz and A. Suzuki, *Nonimaging Fresnel Lenses: Design and Performance of Solar Concentrators*, Springer, Berlin (2001).
6. R. Winston, J. C. Miñano, and P. Benítez, *Nonimaging Optics*, Elsevier Academic Press, Burlington, MA (2005).
7. P. Benítez, M. Hernández, R. Mohedano, J. C. Miñano, and F. Muñoz, "New nonimaging static concentrators for bifacial photovoltaic solar cells," *Nonimaging Optics: Maximum Light Transfer V*, Proc. of the SPIE 3781, 22-29 (1999).
8. R. Winston and J. M. Gordon, "Planar concentrators near the étendue limit," *Opt. Lett.* 30(19), 2617-2619 (2005)